Cryptic prophage-encoded small protein DicB protects *Escherichia coli* from phage infection by inhibiting inner membrane receptor proteins

Preethi T. Ragunathan and Carin K. Vanderpool[a#]

Department of Microbiology, University of Illinois at Urbana-Champaign, Urbana, Illinois, USA[a]

Running title: DicB inhibits mannose phosphotransferase system proteins

[#]Address correspondence to Carin Vanderpool, cvanderp@illinois.edu

Abstract

Bacterial genomes harbor cryptic prophages that have lost genes required for induction, excision from host chromosomes, or production of phage progeny. *Escherichia coli* K12 strains contain a cryptic prophage Qin that encodes a small RNA, DicF, and small protein, DicB, that have been implicated in control of bacterial metabolism and cell division. Since DicB and DicF are encoded in the Qin immunity region, we tested whether these gene products could protect the *E. coli* host from bacteriophage infection. Transient expression of the *dicBF* operon yielded cells that were ~100-fold more resistant to infection by λ phage than control cells, and the phenotype was DicB-dependent. DicB specifically inhibited infection by λ and other phages that use ManYZ membrane proteins for cytoplasmic entry of phage DNA. In addition to blocking ManYZ-dependent phage infection, DicB also inhibited the canonical sugar transport activity of ManYZ. Previous studies demonstrated that DicB interacts with MinC, an FtsZ polymerization inhibitor, causing MinC localization to mid-cell and preventing Z ring formation and cell division. In strains producing mutant MinC proteins that do not interact with DicB, both DicB-dependent phenotypes involving ManYZ were lost. These results suggest that DicB is a pleiotropic regulator of bacterial physiology and cell division, and that these effects are mediated by a key molecular interaction with the cell division protein MinC.

34 **Importance**

35 Temperate bacteriophages can integrate their genomes into the bacterial host chromosome and
36 exist as prophages whose gene products play key roles in bacterial fitness and interactions with
37 eukaryotic host organisms. Most bacterial chromosomes contain “cryptic” prophages that have
38 lost genes required for production of phage progeny but retain genes of unknown function that
39 may be important for regulating bacterial host physiology. This study provides such an example
40 – where a cryptic prophage-encoded product can perform multiple roles in the bacterial host and
41 influence processes including metabolism, cell division, and susceptibility to phage infection.
42 Further functional characterization of cryptic prophage-encoded functions will shed new light on
43 host-phage interactions and their cellular physiological implications.
44

Introduction

Bacteriophages are abundant in the environment with an estimated 10^{31} bacteriophage (phage) particles, and outnumber their bacterial hosts by a factor of 10 to 1 (1, 2). They are found in all ecosystems that harbor bacteria and play a vital role in driving bacterial evolution (3). Based on their lifecycles, phages can be broadly classified as virulent or temperate. Virulent phages use a lytic lifecycle wherein they infect bacterial hosts, use the host cell's resources to make more phage particles and ultimately lyse the cell to release progeny virions into the environment. Temperate phages can grow using a lytic lifecycle, or alternatively can undergo lysogeny – integrating their genomes at a specific attachment site in the host chromosome and remaining stably associated with the host. The bacterium with an integrated phage genome (prophage) is called a lysogen. Changes in host metabolic conditions or external environmental triggers can induce the prophage, which then excises out of the host chromosome and resumes a lytic lifecycle (4, 5).

Nearly half of all sequenced bacterial genomes have been found to contain at least one prophage, with many genomes containing multiple prophages (6). Lysogeny comes at a cost to the bacterial host due to the extra burden of replication of prophage DNA and the threat of lysogen induction which is lethal to the host cell. On the other hand, there are many well-documented examples of lysogenic conversion, where prophage-encoded products confer new and advantageous characteristics on the host (7, 8). Many prophages carry virulence genes that contribute to the pathogenicity of a bacterial host, *e.g.,* phage-encoded Shiga toxin in *E. coli* O157 strains (9), phage-encoded Diphtheria toxin in *Corynebacterium diphtheriae* (10), and neurotoxin in *Clostridium botulinum* (11). Prophage-encoded toxins, host cell invasion factors and serum resistance proteins promote various aspects of the infection processes carried out by bacterial pathogens (7). Another well-documented benefit of prophages is superinfection immunity. In a mixed population of lysogens and other bacteria, if a prophage becomes induced and lyses a host cell, the active phage particles released will only infect and lyse the non-

lysogens, while the lysogens are protected by the prophage-encoded immunity functions (5). Less well-characterized at a mechanistic level are examples of prophage genes that increase the host's ability to grow under different environmental or stress conditions (12–14).

Growing evidence suggests that in many genomes, most of the resident prophages are cryptic (defective), having suffered mutations that leave them unable to excise from the host chromosome, lyse host cells, or produce infectious phage particles (15–18). A recent study identified and characterized orthologous prophages that were integrated in an ancestral host genome and subsequently passed down vertically with the host chromosome in *E. coli* and *Salmonella* (16). Most of these prophages showed evidence of loss of large portions of the original prophage genome, but the remaining genes were under purifying selection (16). These results suggest that certain prophage genes are selected for during host evolution because they encode products that are advantageous to the host under some condition. The cryptic prophages of *E. coli* K12 have been associated with several host phenotypes, including biofilm formation, stress sensitivity, and antibiotic resistance (19). To understand the molecular basis of cryptic prophage-associated phenotypes, functional characterization of prophage-encoded genes is essential.

In *E. coli* K12, the cryptic prophage Qin carries an operon encoding a small protein, DicB, and small RNA (sRNA), DicF, that both function as cell division inhibitors (20–25). The sRNA DicF represses *ftsZ* translation by directly base pairing with the *ftsZ* mRNA near the Shine Dalgarno sequence (24, 25). DicF also regulates other mRNAs that encode a variety of regulatory and metabolic functions (25). The 62-amino acid protein DicB inhibits cell division by directly interacting with MinC and recruiting it to the septum via interactions with the septal protein ZipA, where MinC stimulates depolymerization of the Z ring, resulting in cell filamentation (23, 26–28). The region immediately upstream of the *dicBF* operon encodes *dicA* and *dicC* and is similar in sequence and structural arrangement to the lambdoid phage immunity locus. DicA is analogous to the P22 phage C2 repressor and DicC to the P22 Cro repressor

(29). DicA represses the *dicBF* operon promoter (which is similar to the λ phage P_L promoter) and the natural condition(s) leading to induction of the operon are unknown (29). DicB and DicF are conserved in many strains of *E. coli*, and interestingly, many strains of pathogenic *E. coli* possess multiple cryptic prophages encoding *dicBF* operons (25, 30, 31).

In this study, we have identified a role for the *E. coli dicBF* operon in resistance to bacteriophage infection. Short-term expression of the *dicBF* operon promotes *E. coli* resistance to λ phage infection. The resistance phenotype is primarily attributable to DicB. DicB does not affect λ phage adsorption to host cells. Instead, our results suggest that DicB inhibits injection of λ DNA into the cytoplasm through the inner membrane proteins ManYZ, which are components of the mannose phosphotransferase system. Consistent with an effect of DicB on ManYZ activity, we found that growth of *dicB*-expressing cells on minimal media with mannose as the sole carbon source was strongly inhibited. Our results suggest that products encoded by the *dicBF* operon, found in cryptic prophages in many *E. coli* and *Shigella* strains, can impact bacterial physiology, including by altering cells' susceptibility to bacteriophage infection. We postulate that this may be a common reason why certain cryptic prophage genes are retained in host chromosomes.

Materials and methods

Strain construction and media. All strains and phages used in this study are summarized in Table S1 and oligonucleotides (from Integrated DNA Technologies) are listed in Table S2. The strains used in this study are derivatives of *E. coli* K12 strains MG1655 and BW25113. Chromosomal mutations were constructed using λ red recombination method as described in (32–34) or moved into the required strain background using P1 transduction (35).

Construction of strain DB240, which has a P_{lac} promoter inserted upstream of *ydfA* replacing the native *dicBF* operon promoter, is described in (25). Oligonucleotides O-PR185 and O-PR186 were used to amplify the kanamycin resistance gene from pKD13 and the PCR product was recombined into the chromosome of DB240 using λ red functions produced by

pSIM6 (34). The resulting Δ*dicB*::kan strain was called PR163. The kanamycin cassette was removed using pCP20 to create Δ*dicB*::*scar* strain PR165.

A Δ*manXYZ*::*kan* deletion was moved into DJ624 and DB240 by P1 transduction from YS208 (36) to create PR187 and PR191 respectively. MinC mutants with single amino acid changes E156A and R172A (37) were constructed by first inserting a kan-*araC*-P_{BAD}-*ccdB* PCR product in the *minC* gene in strain DJ624. Oligonucleotides O-PR209/O-PR210 (for E156A) and O-PR205/O-PR206 (for R172A) were used to amplify the kan-*ccdB* region of strain YS243 and the PCR product was recombined into DJ624 (pSIM6) to generate strains PR178 and PR179, respectively. Oligonucleotides O-PR211 and O-PR212 (containing the E156A mutation) were used to amplify a segment of DNA from the control strain DJ480 to generate PCR product with the desired mutations for *minC* E156A and recombined into PR178 pSIM6 to generate strain PR180. Oligonucleotides O-PR213 and O-PR214 (containing the R172A mutation) were used to generate a PCR product similarly with mutations for *minC* R172A and recombined into PR179 pSIM6 to create strain PR181. A P_{lac} promoter replacing the promoter of the *dicBF* operon, was introduced in PR180 and PR181 to generate strains PR182 and PR183 respectively.

E. coli K12 strains were grown in LB medium at 37°C on a rotary shaker. All phage dilutions were made in TM buffer containing 10mM Tris-HCl and 10mM MgSO4, and phage infections were carried out using the same buffer. For phage infections, the top agar was made with equal parts of LB agar and TM buffer, unless specified otherwise (38). Top agar was added to the infection mixture and plated on to LB agar plates.

Phage propagation. New stocks of each phage were prepared as described in Rotman *et al*. (38). Plating cultures were prepared by growing DJ480 in TB medium with 5 mM $MgSO_4$ (and 0.2% maltose exclusively for λ stock preparation) until late log phase, after which an equal amount of TM buffer was added and the mixture was vortexed vigorously. Old phage stocks were titered on the prepared plating culture and plated using top agar, made of equal parts TB

agar and TM buffer, onto TB agar plates and incubated overnight at 37°C. The next day, a single individual plaque was punched out and incubated in TM buffer at room temperature for 1-2 hours with occasional vortexing. Between 10 and 30 µl of the single plaque eluate was mixed with 300 µl of DJ480 plating culture and incubated at 37°C for 15 minutes. 3 ml TB/TM top agar was added and plated onto TB plates for incubation at 37°C. After 3 to 7 hours when the lysis was confluent, the plate was overlaid with 5ml TM buffer overnight at room temperature. The TM buffer containing phage was collected in the morning and 4ml fresh TM buffer was added to the plate and kept at room temperature. After 8 hours, the remaining TM containing phage was collected and the combined eluate was centrifuged to pellet the agar and cells down. The supernatant was transferred into a fresh tube, 50ul chloroform was added and the fresh phage lysate was stored at 4°C.

Efficiency of Plaquing (EOP) assay. The strains used in this experiment were precultured overnight in LB and subcultured in LB medium to ensure all the strains were in the same state of growth when phage infection was carried out. After one hour of sub-culturing (when OD_{600} was ~0.1-0.2), IPTG was added to a final concentration of 0.5 mM to induce the P_{lac} promoter. After one hour with IPTG induction, the cells were washed and resuspended in LB medium. Final OD_{600} was measured, and 1 ml of the culture was centrifuged and resuspended in 1 ml TM buffer. 100 µl of phage dilution was added to 100 µl of bacteria from the previous step and incubated for 10 minutes at 37°C. After 10 minutes, prewarmed 3ml LB top agar was added to the mixture and plated onto LB agar plates. The plates were incubated overnight at 37°C and the plaques were counted. EOP was calculated as: (phage titer on test strain in pfu/ml)/(phage titer on control strain in pfu/ml) (39, 40).

Efficiency of center of infection (ECOI) assay. The strains were prepared for infection as described for EOP assay. The only difference was in the last step of sample preparation, where the cells were resuspended in TM buffer with 0.5 mM IPTG to induce P_{lac}-*dicBF* during phage infection. The procedure followed for the ECOI assay was based on that described in Moineau,

174 *et al*. (41). λ*vir* lysates were added to 500 µl of prepared strains at a multiplicity of infection
175 (MOI) of 0.1 or less and incubated at 37°C for 10 minutes. The infection mixture was washed
176 with TM buffer containing 0.5 mM IPTG to remove unadsorbed phages and resuspended in 500
177 µl of fresh buffer. The infected cells were diluted in TM/IPTG buffer and 100 µl of each dilution
178 of strains was added to 100 µl of DJ480 cells in TM buffer, LB/TM top agar was added to this
179 mixture and plated onto LB agar plates. The plates were incubated overnight at 37°C, and the
180 plaques arising from each individual infection were observed and counted. ECOI is calculated
181 as (number centers of infection/ml from test strain) x 100/(number centers of infection/ml from
182 control strain) (41).
183 **One step growth curve.** The samples were prepared for infection as described for ECOI
184 assays. The one-step growth curve experiment was designed based on (41). After
185 resuspending the cells, λ*vir* was added at an MOI of 0.1 or less to 500 µl of cells and incubated
186 for 10 minutes at 37°C. The infection mixture was washed to remove unadsorbed phages and
187 resuspended in 500 µl of TM buffer with 0.5 mM IPTG. The strains were diluted 1:10,000 for
188 DJ480 and 1:1000 for DB240 (P_{lac}-*dicBF*) to a final volume of 20 ml in LB with 10 mM $MgSO_4$
189 and 0.5 mM IPTG in flasks and incubated in a 37°C water bath. Immediately, 100 µl was
190 withdrawn from the flask and added to 100 µl phage-sensitive DJ480 cells in TM buffer (for lawn
191 formation), added to prewarmed top agar, and plated onto LB agar plates. The first time point
192 was 30 minutes after the start of infection. The same procedure was repeated for each time
193 point. The burst size was calculated as (phage titer at 100 minutes – initial titer at 30 minutes)/
194 initial titer at 30 minutes. The latent period was calculated as the mid-point of the exponential
195 phase of the growth curve (41).
196 **Adsorption assay.** The procedure described above for ECOI assays was followed and after
197 strains were infected with λ*vir* at an MOI of 0.1 and allowed to adsorb for 10 minutes at 37°C,
198 the strains were centrifuged for 5 minutes at 13,000 rpm to pellet cells and adsorbed phage. 100
199 µl of the supernatant was removed and dilutions were made in TM buffer. 10 µl of each dilution

was added to 100 µl DJ480 (phage-sensitive) cells in TM buffer and incubated for 10 minutes at 37°C. This mixture was plated onto LB plates using top agar and incubated overnight at 37°C. Control titer was calculated using the same procedure as above using the same amount of phage required for MOI of 0.1 added to 500 µl TM buffer (no bacteria). Percentage of adsorption was calculated as (control titer – residual titer)*100/ control titer (39, 42).

Growth on minimal medium plates with different sugars. For growth assays, M63 minimal medium plates with sugars (glucose, fructose, mannose, N-acetyl glucosamine, and glucosamine) at a final concentration of 0.2% were prepared without or with 0.025 mM IPTG. The strains were streaked on plates and incubated for 44 hours at 37°C. By visual inspection, strains were scored for growth with +++ denoting normal growth, ++ and + denoting decreasing growth and – as no growth.

Results

Transient induction of the *dicBF* operon protects against λ phage infection. The region of Qin prophage containing the *dicBF* operon (Fig. 1A) resembles the immunity regions of P22 and other lambdoid phages (29). While functions have not been identified for most of the products of the *dicBF* operon, DicB (a small protein) and DicF (a small RNA) have been shown to inhibit cell division (20, 22–25). We showed previously that DicF post-transcriptionally regulates a variety of genes involved in cell division, growth and metabolism (25). Given their position in the immunity region of the prophage genome, and the fact that the characterized gene products impact cell physiology, we hypothesized that products of the *dicBF* operon could cause changes in the host cell that promote resistance to phage infection. We tested this by comparing phage infections of control and *dicBF*-expressing cells. Since the conditions under which the *dicBF* operon is normally expressed are not fully understood, we used an inducible expression system described previously (25) where we replaced the *dicBF* operon promoter with a P_{lac} promoter at the native locus. In addition to the P_{lac}-*dicBF* strain, we used strains with deletions of different genes in the operon (Fig. 1B).

We measured phage infection of these strains by Efficiency of Plaquing (EOP) assays, initially using phage λ. In this assay, the phage is titered on all bacterial strains and the titer in plaque forming units (pfu)/ml is calculated for each strain. The EOP is defined as: phage titer on test strain/phage titer on control strain. The control strain lacked the P_{lac} promoter. Strains with the P_{lac} promoter driving *dicBF* expression were exposed to IPTG for 60 minutes. Then, strains were infected with λ*vir* (a λ mutant that can only complete the lytic cycle during infection of host cells) and plated for titer as described in Materials and Methods. The EOP for the P_{lac}-*dicBF* strain was 0.04 (Fig. 1B), meaning that rate of infection of the *dicBF*-expressing strain was only 4% relative to the control strain. This result suggested that transient expression of the *dicBF* operon conferred resistance to infection by λ*vir*. To further characterize the basis for this phenotype, we deleted *dicF* and *dicB,* singly and in combination because previous studies identified growth or cell division phenotypes associated with these genes (23, 25). Phenotypes of deletion mutants demonstrated that *dicB* played the most prominent role in the resistance phenotype (Fig. 1B). Deletion of *dicB* alone or *dicB* in combination with *dicF* restored the EOP of λ*vir* to nearly that of control. In contrast, deletions of *dicF* alone had a minimal effect on the resistance phenotype (Fig. 1B). We also carried out infections with wild-type λ phage, and saw similar results for EOP on control, *dicBF*-expressing and deletion mutant strains (Fig. S1).

Because previous studies showed that ectopic expression of the *dicBF* operon impairs growth of the host strain, we reasoned that poor growth of test strains could influence the results of EOP assays. To more accurately assess the outcome of a phage infection on cells expressing the *dicBF* operon, we conducted center of infection (COI) assays. For this assay, strains (Fig. 1B) were induced with 0.5 mM IPTG and λ*vir* infection was carried out at a multiplicity of infection (MOI) of 0.1. After adsorption of phage to test strains, the unadsorbed phages were removed by washing and the infected test cells were diluted and mixed with the phage-sensitive control strain. Productive infections of the test strain are detected as plaques (centers of infection) on the phage-sensitive control strain. The efficiency of λ*vir* forming centers

of infection (ECOI) is calculated as (number centers of infection/ml from test strain) x 100/(number centers of infection/ml from control strain). The ECOI for λ*vir* on P$_{lac}$-*dicBF* cells was 3% (Fig. 1C). This result is similar to the results of EOP assays (Fig. 1B), suggesting that the growth characteristics of the P$_{lac}$-*dicBF* test strain did not impact the experimental outcome. Deletion of *dicB*, alone or in combination with *dicF,* restored the ECOI to ~80%. The Δ*dicF* strain gave an ECOI of 5% (Fig. 1C). These results are again consistent with our EOP experiments (Fig.1B) implicating DicB as the major player in the phage resistance phenotype.

The *dicBF* operon promotes resistance against λ, but not other phages. To determine if transient expression of *dicBF* conferred resistance to other phages, we conducted infection experiments using control and P$_{lac}$-*dicBF* strains with nine different lytic and temperate phages (Fig. 2). In this experiment, the EOP of λ*vir* on the P$_{lac}$-*dicBF* strain was 0.016 or 1.6% compared to the control strain, which was the lowest of the nine phages tested (Fig. 2). Partial resistance was observed for T3 phage, which had an EOP of 0.14 on P$_{lac}$-*dicBF* cells. However, the EOP for the remaining seven phages, including phages ϕ80 and HK97, which are closely related to λ, was similar to control cells (Fig. 2). These results suggest DicB does not provide a broad-spectrum of resistance against bacteriophages.

Effect of *dicBF* expression on λ phage growth. The classical experiment to study the growth cycle of phage in bacteria is the one-step growth curve, as described by Ellis and Delbrück (43). They observed a latent period where numbers of phage recovered from infected cells remained low as new phage particles were being synthesized inside the host cell. After the latent period is the “burst” where numbers of infectious phage particles increase rapidly as the phage life cycle is completed and cells are lysed to release mature progeny. We conducted one-step growth curves for λ*vir* on control and *dicBF*-expressing strains, essentially as described above for ECOI experiments over a time course following infection. λ*vir* was added at an MOI of 0.1 to control and P$_{lac}$-*dicBF* cells resuspended in TM buffer. After phage adsorption, the cells were washed to remove unadsorbed phage and the phage-host complexes were diluted into fresh medium with

IPTG (see Materials and Methods). At each time-point, the number of infectious phage particles in each culture was calculated by removing samples and plating for PFU on a phage-sensitive control strain.

As expected based on previous results (Figs. 1B, C), the ECOI for λ*vir* on P_{lac}-*dicBF* cells was reduced by almost 2 logs compared with the control strain at the early time points, and the reduced numbers of phage produced by P_{lac}-*dicBF* cells persisted across the phage growth curve (Fig. 3). The latent period for P_{lac}-*dicBF* cells (75 min.) was ~10 min. longer than for control cells (65 min.) (Fig. 3). The calculated burst sizes were 343 phage/P_{lac}-*dicBF* cell compared to 169 phage/control cell. This increase in burst size in *dicBF*-expressing cells is likely due to filamentation of cells caused by DicB and DicF. It has been shown before that filamenting cells produce more phage than normal size cells (44, 45). Importantly, we observed that the ~3% of phages that escaped DicB-mediated resistance followed a growth curve similar to that of phages growing on control cells. Collectively, these data led us to hypothesize that DicB affects an early step of the phage life cycle like adsorption or DNA injection, since phages that escape this DicB effect complete a relatively normal life-cycle.

The *dicBF* operon does not affect phage adsorption to host cells. To test if expression of the *dicBF* operon affects the first step of phage infection, we tested the ability of λ*vir* to adsorb to host cells expressing this operon. During the ECOI experiment, once phage infection was carried out with cells in TM buffer at an MOI of 0.1 and incubated at 37°C for 10 mins, the phage-cell mixture was centrifuged and the supernatant containing the unadsorbed phages was removed. This supernatant was titered on phage-sensitive control cells by standard plaque assay (residual titer). Control titer was calculated using the same procedure as above, with phage added to TM buffer instead of bacterial cells in the first step of the experiment. The percentage of adsorption was calculated as (control titer – residual titer)*100 / control titer.

The adsorption of λ*vir* to strains expressing the *dicBF* operon was the same as adsorption to the control strain (Table 1). Notably, while λ*vir* and HK97 both adsorb to the same

outer membrane receptor, LamB (46, 47), the effect of *dicBF* expression on the EOP of these two phages is significantly different – with reduced EOP only for λ*vir* (Fig. 2). These observations strongly suggest that DicB does not affect the phage life cycle at the step of adsorption to host cells.

Recombinant λ phages with the host range region of ϕ80 are not affected by DicB. The genomes of λ phage and ϕ80 (a lambdoid phage) have strikingly similar organization, allowing for easy construction of recombinant phage (48, 49). One prominent difference between λ and ϕ80 is their use of different outer and inner membrane receptors. λ uses LamB (outer membrane) and ManYZ (inner membrane) for adsorption and DNA injection respectively (50–54), while ϕ80 uses FhuA (outer membrane) and the TonB complex (inner membrane) (48, 55, 56). The phage genes encoding determinants for utilization of host outer and inner membrane receptors are located in the host range region of lambdoid phage genomes. Our results so far suggest that the DicB-dependent phage resistance phenotype is not due to an effect on adsorption to the outer membrane receptor but might be mediated at another early step of infection such as injection of the phage genome through the inner membrane receptor. To test this idea, we measured phenotypes of control and *dicBF*-expressing cells challenged with recombinant λ phage containing the host range region of ϕ80 (λh80). The λh80 phage carry most of the wild-type λ genome but have an altered host range region specifying use of the ϕ80 outer and inner membrane receptors. To confirm this, we tested the plaquing ability of λh80 phages on wild-type, Δ*fhuA*, Δ*tonB* and Δ*manXYZ E. coli* strains. As expected, the λh80 phages, like ϕ80, did not plaque on Δ*fhuA* and Δ*tonB* strains but formed normal plaques on the Δ*manXYZ* strain (Table S3). Next, we carried out EOP assays using λ*vir* and a panel of recombinant phage with the host range of λ or ϕ80 (Table S1) on control and P_{lac}-*dicBF* cells (Fig. 4). We hypothesized that if DicB mediates resistance to λ phage by impairing injection of phage DNA across the cytoplasmic membrane, then phage with the host range of λ would

329 remain inhibited by DicB, whereas λh80 phage with altered inner membrane receptor specificity
330 would not be impacted by DicB. Results of the EOP assays demonstrate that phage with λ host
331 range remain sensitive to DicB-mediated inhibition while λh80 phages had a similar EOP on
332 P_{lac}-*dicBF* and control cells (Fig. 4). Together with our previous results, this observation
333 suggests that DicB-mediated resistance acts at the level of the inner membrane receptor
334 ManYZ used for λ phage DNA injection into the cytoplasm of *E. coli*. We note that the panel of
335 phages that we tested in this experiment had other genetic differences aside from the different
336 host ranges (Table S1). Only the host range was correlated with susceptibility to DicB-mediated
337 resistance.

338 Phage 434 (53) is another phage that uses ManYZ for injection of DNA through the
339 cytoplasmic membrane (Fig. 5A). Previous studies have shown that *manXYZ* deletion mutants
340 (also known as *pel* mutants) were resistant to infection by λ and phage 434, but not ϕ80 (53). To
341 further test our hypothesis that DicB inhibits phage infection at the level of DNA entry through
342 ManYZ, we tested the ability of λ*vir*, phage 434 and ϕ80 to infect control and *dicBF*-expressing
343 cells in *manXYZ*$^+$ and Δ*manXYZ* backgrounds. We verified that the λ, phage 434 and ϕ80
344 phages plaque as expected on wild-type and strains with mutations in specific receptors (Table
345 S4). As shown above (Fig. 2), ϕ80 plaquing efficiency is not impacted by expression of the
346 *dicBF* operon in a *manXYZ*$^+$ background. The Δ*manXYZ* mutant host also supported wild-type
347 EOPs for ϕ80 plaquing regardless of whether *dicBF* was expressed (Fig. 5B). For λ*vir*, the EOP
348 on P_{lac}-*dicBF* cells was 4% relative to control in *manXYZ*$^+$ cells, whereas the *ΔmanXYZ* host did
349 not support λ*vir* growth (Fig. 5B). The pattern of growth for phage 434 was very similar to that of
350 λ*vir,* with a reduced EOP of ~10% on P_{lac}-*dicBF* cells in the *manXYZ*$^+$ host and no countable
351 plaques on the Δ*manXYZ* host (Fig. 5B). The results of this experiment are consistent with the
352 hypothesis that DicB inhibits the use of the mannose phosphotransferase system proteins,
353 ManYZ, as an inner membrane receptor for productive phage infection.

Growth of *dicBF*-expressing cells is inhibited on plates with mannose as the C source. Our previous results point to the small protein DicB inhibiting the activity of mannose transporter ManYZ proteins with regard to DNA uptake during phage infection. To test whether DicB inhibits the function of these proteins more broadly, we checked the growth of *dicBF*-expressing cells on mannose as the sole C source. For this experiment, we used control, P_{lac}-*dicBF,* and P_{lac}-*dicBF* Δ*dicB* strains. The strains were streaked on M63 minimal plates with different sugars with or without 0.025mM IPTG (to induce *dicBF* expression) and incubated for 44 hours at 37°C (Table 2, Fig. S2). In the absence of inducer, all the strains had near normal growth on the different sugars used. When *dicBF* expression was induced using 0.025mM IPTG, we observed growth inhibition of P_{lac}-*dicBF* cells on mannose and glucosamine, but not on glucose, fructose or N-acetyl glucosamine. Deletion of *dicB* relieved the growth inhibition on mannose and glucosamine. Both mannose and glucosamine sugars are transported via the ManXYZ transporter in *E. coli* (57–59). These results demonstrate that DicB affects growth specifically on substrates of ManYZ. Growth on sugars that are transported by other PTS proteins was unaffected. These data suggest that DicB impacts at least two different functions of ManYZ – uptake of phage DNA during infection and transport of sugar substrates.

MinC mutants that do not interact with DicB lose the phage resistance and sugar phenotypes. The only characterized activity of DicB is inhibition of cell division (20, 60). The mechanism by which DicB impacts cell division requires a protein-protein interaction with MinC, one of the proteins involved in controlling septal ring placement in *E. coli.* MinC is an inhibitor of FtsZ polymerization, and normally MinC concentrations are highest at cell poles so that septum formation is inhibited at polar sites and directed instead to mid-cell (61). Previous work demonstrated that DicB interacts with MinC and brings it to mid-cell via an interaction with ZipA, a septal protein (28). DicB-mediated localization of MinC to cell center inhibits FtsZ polymerization and promotes filamentation (27, 28). To determine if the DicB-MinC interaction is necessary for the DicB-dependent phenotypes we found in this study, we constructed strains

with *minC* mutant alleles that produce MinC proteins that are defective for interaction with DicB. We used two different MinC mutants: MinC R172A, which interacts weakly with DicB, and MinC E156A mutant, which does not interact with DicB (37). In strains expressing these *minC* alleles, DicB has a modest (MinC R172A) or no (MinC E156A) impact on cell division, consistent with their reduced binding to DicB. We used MinC E156A and R172A mutant hosts to test whether the DicB-mediated phage resistance or sugar growth phenotypes required the DicB-MinC interaction.

As observed previously, in the wild-type *minC*$^+$ background, *dicBF*-expressing cells showed reduced EOP for λ*vir* compared to control cells (Fig. 6). However, in the MinC R172A (reduced binding to DicB) strain, the resistance phenotype was diminished – *dicBF* expression in this host gave an EOP of 12% compared to the control strain. In the MinC E156A (abrogated binding to DicB) background, the EOP of λ*vir* on *dicBF*-expressing cells was very similar to the control strain (Fig. 6). These results suggested that the DicB-MinC interaction is required for the DicB-mediated resistance to λ phage infection. The same strains were grown on M63 minimal plates with different sugars without or with 0.025mM IPTG to induce the *dicBF* operon. As shown above, in the wild-type *minC*$^+$ background, expression of *dicBF* inhibited growth on plates with mannose and glucosamine, but not on plates with glucose (Table 3). In contrast, *dicBF* expression in *minC* mutant strains (E156A and R172A) did not inhibit growth on any of the sugars tested (Table 3). Collectively, these data indicate that the new DicB-associated phenotypes we have identified – phage resistance and inhibition of growth on sugars that are transported by ManYZ – require the previously defined molecular mechanism of DicB interaction with the host protein MinC.

Discussion

The existence of cryptic or defective prophages on bacterial chromosomes was discovered long ago (4), but their potential beneficial functions for host cells are still coming to light. In part, this is because we do not know the functions of the majority of genes encoded on

406 these prophages. In this study, we have identified a new functional role for the cryptic prophage-
407 encoded protein DicB in *E. coli* K12. We showed that induction of the *dicBF* operon makes cells
408 resistant to infection by phages that use the ManYZ PTS proteins as inner membrane receptors
409 for DNA injection (Figs. 1, 5). DicB, a 62-amino acid protein encoded by the *dicBF* operon, plays
410 the primary role in conferring this phage resistance phenotype (Fig. 1). Our results are
411 consistent with the model that DicB inhibits phage DNA injection through the mannose
412 transporter proteins ManYZ (Figs. 4, 5). The DicB effect on ManYZ also inhibits ManYZ-
413 dependent transport of sugar substrates (Tables 2, 3), suggesting that DicB affects the general
414 structure or function of these transport proteins. Previous work demonstrated that DicB inhibits
415 cell division by interacting with and affecting localization and activity of the cell division proteins
416 MinC and FtsZ (23, 26–28). In this study, we found that the DicB-associated phage resistance
417 and sugar utilization phenotypes are dependent on DicB-MinC interactions (Fig. 6).
418 Prior to this work, the only known function of DicB was inhibition of cell division. DicB
419 directly interacts with MinC of the Min system, which consists of the proteins MinC, MinD and
420 MinE, which play a role in spatial positioning of the FtsZ ring at mid-cell for cell division. MinC is
421 a negative regulator of FtsZ polymerization, and in *E. coli* MinC oscillates between the two cell
422 poles (driven by MinD and MinE) in order to inhibit Z ring assembly at the poles (62, 63).
423 However, when DicB is expressed, a DicB-MinC complex is formed which interacts with the
424 septal ring component ZipA and stimulates Z ring depolymerization at mid-cell leading to cell
425 filamentation (28). Both activities of DicB, cell division inhibition and the ManYZ inhibition
426 phenotypes reported in this study, involve interaction with MinC. These results imply a
427 previously unsuspected link between the Min system or other components of the cell division
428 machinery and the mannose PTS. A few studies have examined localization of various PTS
429 proteins. The general PTS proteins, EI and HPr, were found to localize primarily to cell poles
430 (64, 65). Localization of EII sugar permeases has been less studied, but there is recent
431 evidence that these proteins cluster together around the cell membrane (66). It will be

interesting in future work to explore the subcellular localization of ManYZ and examine if or how it is impacted by MinC and DicB.

It is clear that active prophages can protect their hosts from superinfection by other phages (67, 68). One of the earliest identified phage resistance mechanisms is called superinfection exclusion, which can occur by a number of different mechanisms (67, 68). One mechanism of superinfection exclusion is mediated by prophage-encoded proteins that block entry of a superinfecting phage's DNA by mechanisms that are not well defined, but may involve modifying the activity or function of inner membrane receptors (67). For example, protein gp15 of HK97 prophage inhibits superinfection by HK97 phage by preventing phage DNA entry through the PtsG inner membrane receptor (47, 69). SieA is an inner membrane protein encoded by the P22 prophage of *Salmonella typhimurium* that prevents infection by P22, L, MG178, and MG40 phages by inhibiting DNA entry into the cytoplasm (70, 71). The P1 prophage-encoded Sim protein was also shown to confer superinfection immunity against P1 and few other phages by an unknown mechanism that occurs after adsorption of the infecting phage (72). While these examples illustrate superinfection exclusion by active prophages, our results suggest that in at least some cases defective prophages can play similar roles in protecting their hosts from phage infection.

E. coli strains have several defective prophages residing on their chromosomes, many of which have undergone extensive deletions since their original integration (16). There is evidence that many of the genes remaining on the cryptic prophages, including the core phage genes which code for tail and lysis proteins, are under strong purifying selection, implying that these genes now perform functions beneficial to the host (16). *E. coli* K12 has 9 defective prophages, 8 of which do not respond to conditions that usually induce an active prophage (19). Some of these prophages have lost genes important for excision from the host chromosome. For example, CP4-44 prophage entirely lacks an integrase, Qin prophage has an inactive integrase and DLP12 prophage has lost part of the excisionase gene (19, 73). Pathogenic *E.*

458 *coli* O157:H7 strain Sakai harbors 18 prophages and 17 of these were found to have defects in
459 the prophage genes required for excision and morphogenesis (15). Though not fully functional,
460 three of these 18 defective prophages carry virulence factors and were capable of packaging
461 and transferring their DNA to *E. coli* K12 (15). These observations demonstrate that even
462 though defective prophages have undergone significant genetic changes through their life
463 history with the host, some retain functions that allow them to continue acting as gene-transfer
464 agents.

465 It has been speculated that another beneficial role of defective prophages could be
466 encoding functions that are important for host cell adaptation to stress conditions. In a study by
467 Wang *et al*. (19), defective prophages of *E. coli* K12 were shown to increase resistance to
468 environmental stresses like oxidative stress, osmotic stress, and to certain antibiotics like
469 quinolones and beta-lactams. This study reported that Δ*qin* derivatives of the parent strain were
470 more sensitive to beta-lactam antibiotics and that Δ*dicB* strains showed greater sensitivity to
471 azlocillin and nalidixic acid (19). We constructed Δ*qin* and Δ*dicB* strains and examined
472 sensitivity to nalidixic acid and ampicillin, and we found no differences in sensitivity between
473 parent strains and mutants (data not shown). It is possible that phenotypes vary with strain
474 background – our strains are MG1655 derivatives and Wang, *et al*., used BW25113 (19).

475 Identifying the signals or conditions that induce prophage genes will be key to
476 understanding their physiological roles in host cells. We have exposed our strains to various
477 conditions that are known to induce prophage gene expression, including DNA damage,
478 starvation, and exposure to antibiotics, and have not yet identified conditions that substantially
479 induce transcription from the native *dicBF* promoter (data not shown). Another study (74),
480 reported that *E. coli* K12 MG1655 cells undergo DicF-dependent filamentation under
481 anaerobic conditions (growth in large volume anaerobic fermenters). The authors of this study
482 suggest that stability of DicF is differentially regulated such that it is more stable under
483 anaerobic growth conditions and degraded faster under aerobic conditions. A very recent

484 study found that four DicF orthologs encoded by different prophages in *E. coli* O157:H7 are
485 produced under microaerobic growth conditions (31). These DicF sRNAs promote low oxygen-
486 responsive virulence gene expression via base pairing-mediated regulation of a key virulence
487 transcription factor. These studies suggest that in at least some *E. coli* strain backgrounds,
488 oxygen is an important signal for modulation of *dicBF* operon transcription or DicF mRNA
489 stability. However, we have not observed any DicF- or DicB-mediated filamentation of
490 MG1655 cells grown in small volume LB liquid cultures in an anaerobic chamber (data not
491 shown), so we speculate that additional signals or conditions might contribute to *dicBF* operon
492 expression in our host strain background.

493 Previous studies from our lab characterized the mRNA target regulon of DicF (25). In
494 addition to the previously discovered DicF target *ftsZ* mRNA, we found that DicF base pairs with
495 and represses translation of *xylR*, *pykA* and *manXYZ* mRNAs, encoding the xylose repressor,
496 pyruvate kinase, and mannose PTS components, respectively (25, 75). Thus, the *dicBF* operon
497 encodes a base pairing-dependent sRNA regulator (DicF) and a small protein (DicB) that act at
498 different levels to inhibit the synthesis and activity of a PTS sugar transporter (ManXYZ). This is
499 strikingly similar to the regulation of the glucose PTS (*ptsG,* enzyme $IICB^{Glc}$) by the dual-
500 function sRNA SgrS and the small protein it encodes, SgrT. SgrS base pairs with and
501 represses translation of *ptsG* mRNA (76, 77), while SgrT inhibits PtsG activity at a post-
502 translational level (78–80). Perhaps regulation of PTS enzyme synthesis and activity by
503 sRNAs and small proteins is a common mechanism for post-transcriptional control of these
504 systems. Future studies on the multitude of sRNAs and small proteins encoded on prophages
505 and bacterial chromosomes promise to reveal more surprising connections between phages
506 and their hosts.

507 **Acknowledgements**

508 We thank Jeffrey Gardner, Andrei Kuzminov, Alan Davidson, and Sankar Adhya for their
509 generous gifts of various phages which were critical for our experiments. We also thank Nadim

Majdalani and John Cronan for providing strains. We are grateful to James Slauch for his help and advice with the design of phage experiments. Finally, we would like to express our thanks to former and current Vanderpool and Slauch lab members for thought-provoking discussions.

This work was supported by the National Institutes of Health (R01 GM092830) and the University of Illinois Department of Microbiology Alice Helm Fellowship to P.T.R.

References

1. Brüssow H, Hendrix RW. 2002. Phage genomics: small is beautiful. Cell 108:13–16.
2. Keen EC. 2015. A century of phage research: bacteriophages and the shaping of modern biology. Bioessays 37:6–9.
3. Hayes S, Mahony J, Nauta A, van Sinderen D. 2017. Metagenomic approaches to assess bacteriophages in various environmental niches. Viruses 9:127.
4. Casjens S. 2003. Prophages and bacterial genomics: what have we learned so far? Mol Microbiol 49:277–300.
5. Harrison E, Brockhurst MA. 2017. Ecological and evolutionary benefits of temperate phage: what does or doesn't kill you makes you stronger. BioEssays 39:1700112.
6. Touchon M, Bernheim A, Rocha EPC. 2016. Genetic and life-history traits associated with the distribution of prophages in bacteria. ISME J 10:2744–2754.
7. Fortier L-C, Sekulovic O. 2013. Importance of prophages to evolution and virulence of bacterial pathogens. Virulence 4:354–365.
8. Brussow H, Canchaya C, Hardt W-D. 2004. Phages and the evolution of bacterial pathogens: from genomic rearrangements to lysogenic conversion. Microbiol Mol Biol Rev 68:560–602.
9. Herold S, Karch H, Schmidt H. 2004. Shiga toxin-encoding bacteriophages – genomes in motion. Int J Med Microbiol 294:115–121.
10. Freeman VJ. 1951. Studies on the virulence of bacteriophage-infected strains of *Corynebacterium diphtheriae*. J Bacteriol 61:675–688.
11. Eklund MW, Poysky FT, Reed SM, Smith CA. 1971. Bacteriophage and the toxigenicity of *Clostridium botulinum* type C. Science 172:480–482.
12. Edlin G, Lin L, Bitner R. 1977. Reproductive fitness of P1, P2, and Mu lysogens of *Escherichia coli*. J Virol 21:560–564.
13. Zeng Z, Liu X, Yao J, Guo Y, Li B, Li Y, Jiao N, Wang X. 2016. Cold adaptation regulated

559 by cryptic prophage excision in *Shewanella oneidensis*. ISME J 10:2787–2800.
560 14. Gödeke J, Paul K, Lassak J, Thormann KM. 2010. Phage-induced lysis enhances biofilm
561 formation in *Shewanella oneidensis* MR-1. ISME J 5:613–626.
562 15. Asadulghani M, Ogura Y, Ooka T, Itoh T, Sawaguchi A, Iguchi A, Nakayama K, Hayashi
563 T. 2009. The defective prophage pool of *Escherichia coli* O157: prophage-prophage
564 interactions potentiate horizontal transfer of virulence determinants. PLoS Pathog
565 5:e1000408.
566 16. Bobay L-M, Touchon M, Rocha EPC. 2014. Pervasive domestication of defective
567 prophages by bacteria. Proc Natl Acad Sci U S A 111:12127–12132.
568 17. Matos RC, Lapaque N, Rigottier-Gois L, Debarbieux L, Meylheuc T, Gonzalez-Zorn B,
569 Repoila F, de Lopes MF, Serror P. 2013. *Enterococcus faecalis* prophage dynamics and
570 contributions to pathogenic traits. PLoS Genet 9:e1003539.
571 18. Ramisetty BCM, Sudhakari PA. 2019. Bacterial 'grounded' prophages: hotspots for
572 genetic renovation and innovation. Front Genet 10:65.
573 19. Wang X, Kim Y, Ma Q, Hong SH, Pokusaeva K, Sturino JM, Wood TK. 2010. Cryptic
574 prophages help bacteria cope with adverse environments. Nat Commun 1:147.
575 20. Béjar S, Bouché JP. 1985. A new dispensable genetic locus of the terminus region
576 involved in control of cell division in *Escherichia coli*. Mol Gen Genet 201:146–150.
577 21. Bouché F, Bouché J-P. 1989. Genetic evidence that DicF, a second division inhibitor
578 encoded by the *Escherichia coli dicB* operon, is probably RNA. Mol Microbiol 3:991–994.
579 22. Labie C, Bouché F, Bouché JP. 1989. Isolation and mapping of *Escherichia coli*
580 mutations conferring resistance to division inhibition protein DicB. J Bacteriol 171:4315–
581 4319.
582 23. de Boer PA, Crossley RE, Rothfield LI. 1990. Central role for the *Escherichia coli minC*
583 gene product in two different cell division-inhibition systems. Proc Natl Acad Sci U S A
584 87:1129–1133.

585 24. Tétart F, Bouché J -P. 1992. Regulation of the expression of the cell-cycle gene *ftsZ* by
586 DicF antisense RNA. Division does not require a fixed number of FtsZ molecules. Mol
587 Microbiol 6:615–620.
588 25. Balasubramanian D, Ragunathan PT, Fei J, Vanderpool CK. 2016. A prophage-encoded
589 small RNA controls metabolism and cell division in *Escherichia coli*. mSystems 1:e00021-
590 15.
591 26. Labie C, Bouché F, Bouché JP. 1990. Minicell-forming mutants of *Escherichia coli*:
592 suppression of both DicB- and MinD-dependent division inhibition by inactivation of the
593 *minC* gene product. J Bacteriol 172:5852–5855.
594 27. Johnson JE, Lackner LL, de Boer PAJ. 2002. Targeting of (D)MinC/MinD and
595 (D)MinC/DicB complexes to septal rings in *Escherichia coli* suggests a multistep
596 mechanism for MinC-mediated destruction of nascent FtsZ rings. J Bacteriol 184:2951–
597 2962.
598 28. Johnson JE, Lackner LL, Hale CA, De Boer PAJ. 2004. ZipA is required for targeting of
599 ^{D}MinC/DicB, but not ^{D}MinC/MinD, complexes to septal ring assemblies in *Escherichia*
600 *coli*. J Bacteriol 186:2418–2429.
601 29. Béjar S, Bouché F, Bouché JP. 1988. Cell division inhibition gene *dicB* is regulated by a
602 locus similar to lamboid bacteriophage immunity loci. Mol Gen Genet 212:11–19.
603 30. Faubladier M, Bouché JP. 1994. Division inhibition gene *dicF* of *Escherichia coli* reveals a
604 widespread group of prophage sequences in bacterial genomes. J Bacteriol 176:1150–
605 1156.
606 31. Melson EM, Kendall MM. 2019. The sRNA DicF integrates oxygen sensing to enhance
607 enterohemorrhagic *Escherichia coli* virulence via distinctive RNA control mechanisms.
608 Proc Natl Acad Sci U S A 116:14210–14215.
609 32. Yu D, Ellis HM, Lee E-C, Jenkins NA, Copeland NG, Court DL. 2000. An efficient
610 recombination system for chromosome engineering in *Escherichia coli*. Proc Natl Acad

611 Sci U S A 97:5978–5983.

612 33. Datsenko KA, Wanner BL. 2000. One-step inactivation of chromosomal genes in
613 *Escherichia coli* K-12 using PCR products. Proc Natl Acad Sci U S A 97:6640–6645.

614 34. Chan W, Costantino N, Li R, Lee SC, Su Q, Melvin D, Court DL, Liu P. 2007. A
615 recombineering based approach for high-throughput conditional knockout targeting vector
616 construction. Nucleic Acids Res 35:e64.

617 35. Miller J. 1972. Experiments in molecular genetics. Cold Spring Harbor Laboratory, Cold
618 Spring Harbor, NY.

619 36. Sun Y, Vanderpool CK. 2013. Physiological consequences of multiple-target regulation
620 by the small RNA SgrS in *Escherichia coli*. J Bacteriol 195:4804–4815.

621 37. Zhou H, Lutkenhaus J. 2005. MinC mutants deficient in MinD- and DicB-mediated cell
622 division inhibition due to loss of interaction with MinD, DicB, or a septal component. J
623 Bacteriol 187:2846–2857.

624 38. Rotman E, Amado L, Kuzminov A. 2010. Unauthorized horizontal spread in the laboratory
625 environment: the tactics of Lula, a temperate lambdoid bacteriophage of *Escherichia coli*.
626 PLoS One 5:e11106.

627 39. Sanders ME, Klaenhammer TR. 1980. Restriction and modification in group N
628 streptococci: effect of heat on development of modified lytic bacteriophage. Appl Environ
629 Microbiol 40:500–506.

630 40. Domingues S, McGovern S, Plochocka D, Santos MA, Ehrlich SD, Polard P, Chopin M-C.
631 2008. The lactococcal abortive infection protein AbiP is membrane-anchored and binds
632 nucleic acids. Virology 373:14–24.

633 41. Moineau S, Durmaz E, Pandian S, Klaenhammer TR. 1993. Differentiation of two abortive
634 mechanisms by using monoclonal antibodies directed toward lactococcal bacteriophage
635 capsid proteins. Appl Environ Microbiol 59:208–212.

636 42. Stockdale SR, Mahony J, Courtin P, Chapot-Chartier M-P, van Pijkeren J-P, Britton RA,

637 Neve H, Heller KJ, Aideh B, Vogensen FK, van Sinderen D. 2013. The lactococcal
638 phages Tuc2009 and TP901-1 incorporate two alternate forms of their tail fiber into their
639 virions for infection specialization. J Biol Chem 288:5581–5590.
640 43. Ellis EL, Delbrück M. 1939. The growth of bacteriophage. J Gen Physiol 22:365–84.
641 44. Hadas H, Einav M, Fishov I, Zaritsky A. 1997. Bacteriophage T4 development depends
642 on the physiology of its host *Escherichia coli*. Microbiology 143:179–185.
643 45. Comeau AM, Tétart F, Trojet SN, Prère M-F, Krisch HM. 2007. Phage-Antibiotic Synergy
644 (PAS): *β*-lactam and quinolone antibiotics stimulate virulent phage growth. PLoS One
645 2:e799.
646 46. Dhillon EKS, Dhillon TS, Lai ANC, Linn S. 1980. Host range, immunity and antigenic
647 properties of lambdoid coliphage HK97. J Gen Virol 50:217–220.
648 47. Cumby N, Reimer K, Mengin-Lecreulx D, Davidson AR, Maxwell KL. 2015. The phage tail
649 tape measure protein, an inner membrane protein and a periplasmic chaperone play
650 connected roles in the genome injection process of *E. coli* phage HK97. Mol Microbiol
651 96:437–447.
652 48. Rybchin VN. 1984. Genetics of bacteriophage *φ*80 - a review. Gene 27:3-11.
653 49. Rotman E, Kouzminova E, Plunkett G, Kuzminov A. 2012. Genome of
654 Enterobacteriophage Lula/phi80 and insights into its ability to spread in the laboratory
655 environment. J Bacteriol 194:6802–6817.
656 50. Randall Hazelbauer L, Schwartz M. 1973. Isolation of the bacteriophage lambda receptor
657 from *Escherichia coli*. J Bacteriol 116:1436–1446.
658 51. Boos W, Shuman H. 1998. Maltose/maltodextrin system of *Escherichia coli*: transport,
659 metabolism, and regulation. Microbiol Mol Biol Rev 62:204–229.
660 52. Esquinas-Rychen M, Erni B. 2001. Facilitation of bacteriophage lambda DNA injection by
661 inner membrane proteins of the bacterial phosphoenol-pyruvate: carbohydrate
662 phosphotransferase system (PTS). J Mol Microbiol Biotechnol 3:361–370.

663 53. Scandella D, Arber W. 1974. An *Escherichia coli* mutant which inhibits the injection of
664 phage λ DNA. Virology 58:504–513.
665 54. Erni B, Zanolari B, Kocher HP. 1987. The mannose permease of *Escherichia coli* consists
666 of three different proteins. Amino acid sequence and function in sugar transport, sugar
667 phosphorylation, and penetration of phage lambda DNA. J Biol Chem 262:5238–5247.
668 55. Hancock REW, Braun V. 1976. Nature of the energy requirement for the irreversible
669 adsorption of bacteriophages T1 and *φ*80 to *Escherichia coli*. J Bacteriol 125:409–415.
670 56. Braun V. 1985. The iron-transport systems of *Escherichia coli*, p. 617–652. *In* Martonosi,
671 AN (ed.), The Enzymes of Biological Membranes. Springer, Boston, MA.
672 57. Postma PWW, Lengeler JWW, Jacobson GRR. 1993.
673 Phosphoenolpyruvate:carbohydrate phosphotransferase systems of bacteria. Microbiol
674 Rev 57:543–594.
675 58. Plumbridge J. 2000. A mutation which affects both the specificity of PtsG sugar transport
676 and the regulation of *ptsG* expression by Mlc in *Escherichia coli*. Microbiology 146:2655–
677 2663.
678 59. Curtis SJ, Epstein W. 1975. Phosphorylation of D-glucose in *Escherichia coli* mutants
679 defective in glucosephosphotransferase, mannosephosphotransferase, and glucokinase.
680 J Bacteriol 122:1189–1199.
681 60. Cam K, Béjar S, Gil D, Bouché JP. 1988. Identification and sequence of gene *dicB*:
682 translation of the division inhibitor from an in-phase internal start. Nucleic Acids Res
683 16:6327–6338.
684 61. Margolin W. 2000. Themes and variations in prokaryotic cell division. FEMS Microbiol
685 Rev 24:531–548.
686 62. Hu Z, Mukherjee A, Pichoff S, Lutkenhaus J. 1999. The MinC component of the division
687 site selection system in *Escherichia coli* interacts with FtsZ to prevent polymerization.
688 Proc Natl Acad Sci U S A 96:14819–14824.

689 63. Pichoff S, Lutkenhaus J. 2001. *Escherichia coli* division inhibitor MinCD blocks septation
690 by preventing Z-ring formation. J Bacteriol 183:6630–6635.
691 64. Lopian L, Elisha Y, Nussbaum-Shochat A, Amster-Choder O. 2010. Spatial and temporal
692 organization of the *E. coli* PTS components. EMBO J 29:3630–3645.
693 65. Govindarajan S, Elisha Y, Nevo-Dinur K, Amster-Choder O. 2013. The general
694 phosphotransferase system proteins localize to sites of strong negative curvature in
695 bacterial cells. MBio 4:e00443-13.
696 66. Martins GB, Giacomelli G, Goldbeck O, Seibold GM, Bramkamp M. 2019. Substrate-
697 dependent cluster density dynamics of *Corynebacterium glutamicum* phosphotransferase
698 system permeases. Mol Microbiol 111:1335–1354.
699 67. Labrie SJ, Samson JE, Moineau S. 2010. Bacteriophage resistance mechanisms. Nat
700 Rev Microbiol 8:317–327.
701 68. Bondy-Denomy J, Davidson AR. 2014. When a virus is not a parasite: the beneficial
702 effects of prophages on bacterial fitness. J Microbiol 52:235–242.
703 69. Cumby N, Edwards AM, Davidson AR, Maxwell KL. 2012. The bacteriophage HK97 gp15
704 moron element encodes a novel superinfection exclusion protein. J Bacteriol 194:5012–
705 5019.
706 70. Susskind MM, Botstein D, Wright A. 1974. Superinfection exclusion by P22 prophage in
707 lysogens of *Salmonella typhimurium*: III. Failure of superinfecting phage DNA to enter
708 *sieA*$^{+}$ lysogens. Virology 62:350–366.
709 71. Hofer B, Ruge M, Dreiseikelmann B. 1995. The superinfection exclusion gene (*sieA*) of
710 bacteriophage P22: identification and overexpression of the gene and localization of the
711 gene product. J Bacteriol 177:3080–3086.
712 72. Kliem M, Dreiseikelmann B. 1989. The superimmunity gene *sim* of bacteriophage P1
713 causes superinfection exclusion. Virology 171:350–355.
714 73. Campbell AM. 1998. Prophages and cryptic prophages, p. 23–29. *In* de Bruijn, FJ,

Lupski, JR, Weinstock, GM (eds.), Bacterial Genomes. Springer, Boston, MA.

74. Murashko ON, Lin-Chao S. 2017. *Escherichia coli* responds to environmental changes using enolasic degradosomes and stabilized DicF sRNA to alter cellular morphology. Proc Natl Acad Sci U S A 114:E8025–E8034.

75. Azam MS, Vanderpool CK. 2017. Translational regulation by bacterial small RNAs via an unusual Hfq-dependent mechanism. Nucleic Acids Res 46:2585–2599.

76. Vanderpool CK, Gottesman S. 2004. Involvement of a novel transcriptional activator and small RNA in post-transcriptional regulation of the glucose phosphoenolpyruvate phosphotransferase system. Mol Microbiol 54:1076–1089.

77. Balasubramanian D, Vanderpool CK. 2013. Deciphering the interplay between two independent functions of the small RNA regulator SgrS in *Salmonella*. J Bacteriol 195:4620–4630.

78. Wadler CS, Vanderpool CK. 2007. A dual function for a bacterial small RNA: SgrS performs base pairing-dependent regulation and encodes a functional polypeptide. Proc Natl Acad Sci U S A 104:20454–20459.

79. Lloyd CR, Park S, Fei J, Vanderpool CK. 2017. The small protein SgrT controls transport activity of the glucose-specific phosphotransferase system. J Bacteriol 199:e00869-16.

80. Kosfeld A, Jahreis K. 2012. Characterization of the interaction between the small regulatory peptide SgrT and the $EIICB^{Glc}$ of the glucose-phosphotransferase system of *E. coli* K-12. Metabolites 2:756–774.

	Control	P_{lac}-*dicBF*	P_{lac}-*dicBF* Δ*dicB*	P_{lac}-*dicBF* Δ*dicF*	P_{lac}-*dicBF* Δ*dicF* Δ*dicB*
% adsorption	99	99	99	99	99
Standard error (+/-)	0.22	0.25	0.69	0.23	0.15

Table 1. The *dicBF* operon does not affect phage adsorption to host cells. The strains used in this experiment are control (DJ480), P_{lac}-*dicBF* (DB240), P_{lac}-*dicBF* Δ*dicB* (DB243), P_{lac}-*dicBF* Δ*dicF* (DB247) and P_{lac}-*dicBF* Δ*dicF* Δ*dicB* (DB248). Cells were infected at an MOI of 0.1 with λ*vir* and allowed to adsorb for 10 mins. at 37°C. After adsorption, the samples were centrifuged and the supernatant containing the unadsorbed phages were titered on phage sensitive cells for quantification (residual titer). Control titer was calculated by carrying out the assay with TM buffer, without bacterial cells. The percentage of adsorption was calculated as (control titer-residual titer)*100/ control titer. Standard error was calculated as standard deviation of values from three biological replicates.

Carbon Source	Control		P_{lac}-*dicBF*		P_{lac}-*dicBF* Δ*dicB*	
	Uninduced	Induced	Uninduced*	Induced	Uninduced*	Induced
Mannose	+++	+++	++	+	+++	+++
Glucose	+++	+++	+++	+++	+++	+++
Glucosamine	+++	+++	++	+	+++	+++
Fructose	+++	+++	+++	+++	+++	+++
N-acetyl glucosamine	+++	+++	+++	+++	+++	+++

Table 2. Growth of *dicBF* expressing cells is inhibited on plates with mannose as the C source. The strains were streaked on M63 minimal medium with 0.2% sugars as C source without or with 0.025mM IPTG and incubated for 44 hours at 37°C. The strains used were control (DJ624), P_{lac}-*dicBF* (DB240) and P_{lac}-*dicBF* Δ*dicB* (PR165). +++ indicates normal growth, ++ and + indicates decremental growth. * denotes that the P_{lac} promoter is leaky and we suspect low level expression of the *dicBF* operon even at 0mM IPTG.

	Glucose		Mannose		Glucosamine	
	Uninduced	Induced	Uninduced	Induced	Uninduced	Induced
Control	+++	+++	+++	+++	+++	+++
P_{lac}-*dicBF*	+++	+++	++	+	++	+
Control *minC* R172A	+++	+++	+++	+++	+++	+++
P_{lac}-*dicBF* *minC* R172A	+++	+++	+++	+++	+++	+++
Control *minC* E156A	+++	+++	+++	+++	+++	+++
P_{lac}-*dicBF* *minC* E156A	+++	+++	+++	+++	+++	+++

Table 3. MinC mutants that do not interact with DicB regain ability to grow on Mannose and Glucosamine. The strains were streaked on M63 minimal medium plates with 0.2% sugars and 0.025mM IPTG to induce *dicBF* operon. The plates were incubated for 44 hours at 37°C. The strains used in this experiment are control (DJ624), P_{lac}-*dicBF* (DB240), control *minC* R172A (PR181), P_{lac}-*dicBF* *minC* R172A (PR183), control *minC* E156A (PR180) and P_{lac}-*dicBF* *minC* E156A (PR182). +++ indicates normal growth, ++ and + indicates decremental growth. The P_{lac} promoter is leaky and we suspect low level expression of the *dicBF* operon even at 0mM IPTG.

798 **Figure 1. Transient induction of the *dicBF* operon protects against λ*vir* infection.** (A) The
799 *dicBF* locus on Qin prophage of *E. coli* K12. The red arrow indicates where P_{lac} is inserted on
800 the chromosome, replacing the native *dicBp* promoter. (B) Efficiency of Plaquing (EOP) is
801 defined as (λ*vir* titer on the test strain)/ (λ*vir* titer on the control strain). Strains used in this
802 experiment were: control (DJ480), P_{lac}-*dicBF* (DB240), P_{lac}-*dicBF* Δ*dicB* (PR165), P_{lac}-*dicBF*
803 Δ*dicF* (DB247) and P_{lac}-*dicBF* Δ*dicF* Δ*dicB* (DB248). All strains were grown to the same state of
804 growth with the *dicBF* operon induced with 0.5 mM IPTG for 60 minutes. The inducer was
805 washed off, the strains were resuspended in TM buffer, infected with λ*vir* and plated to calculate
806 titer. Error bars were calculated as standard deviation of values from three biological replicates.
807 (C) Efficiency of center of infection (ECOI) is calculated as (number of infectious centers/ml from
808 test strain)* 100/(number of infectious centers/ml from control strain). The strains used in this
809 experiment are control (DJ480), P_{lac}-*dicBF* (DB240), P_{lac}-*dicBF* Δ*dicB* (DB243), P_{lac}-*dicBF* Δ*dicF*
810 (DB247) and P_{lac}-*dicBF* Δ*dicF* Δ*dicB* (DB248). The cells were grown with induction of the *dicBF*
811 operon with 0.5 mM IPTG and infected with λ*vir* at an MOI of 0.1. The unadsorbed phages were
812 removed, the phage-host complex was added to phage sensitive cells (DJ480) and plated onto
813 LB agar for counting plaques (infectious centers). Error bars were calculated as standard
814 deviation of values from three biological replicates.
815 **Figure 2. The *dicBF* operon confers resistance against λ phage but not other phages.** For
816 each of the nine phages, titer in terms of pfu/ml was calculated by infection of control (DJ480)
817 and P_{lac}-*dicBF* (DB240) cells. The cells were prepared for infection and the EOP was calculated
818 for each phage as described for Fig.1B. Error bars were calculated as standard deviation of
819 values from three biological replicates.
820 **Figure 3. One step growth curve of λ*vir* control and P_{lac}-*dicBF* cells.** The cells were grown
821 with induction of the *dicBF* operon and infection was carried out an MOI of 0.1, similar to the
822 center of infection assay. After removing unadsorbed phages, the cells were diluted in LB
823 medium (with IPTG to induce the *dicBF* operon) and incubated at 37°C for the entire duration of

the growth curve. At each time point starting at 30 minutes from the start of infection, samples were removed and added to the phage-sensitive strain (DJ480), and plated to count plaques. Burst size was calculated as (phage titer at 100 minutes - initial titer at 30 minutes)/initial titer at 30 minutes. Latent period was calculated as the time at the mid-point of the exponential phase of the curve. Error bars were calculated as standard deviation of values from three biological replicates.

Figure 4. λ phage with the host range of ϕ80 is not affected by DicB. Recombinant λ phages with either the λ or ϕ80 host range were plaqued on control (DJ480) or P_{lac}-*dicBF* (DB240) cells. Phage names from left to right are: 185, 148, 169, 173, 158, 138 and λ*vir* (see Table S1 for phage genotypes). The cells were prepared for infection and the EOP was calculated for each phage as described for Fig. 1B. Error bars were calculated as standard deviation of values from three biological replicates.

Figure 5. Phage 434 plaquing on ManYZ^{+} strains is inhibited by the *dicBF* operon. (A) Outer and inner membrane receptor specificity of phages λ*vir*, 434 and ϕ80. (B) EOP assay was carried out by preparing cells and calculating titer of phages on the different strains as described in Fig.1B. The strains used in this experiment are control (DJ624), P_{lac}-*dicBF* (DB240), control Δ*manXYZ*::kan (PR187) and P_{lac}-*dicBF* Δ*manXYZ*::kan (PR191). EOP of phages for each strain is calculated with respect to the control strain in the same background. Error bars were calculated as standard deviation of values from three biological replicates. * denotes strains for which plaques could not be counted.

Figure 6. MinC mutants that do not interact with DicB lose the phage resistance effect. The cells were grown with induction of the *dicBF* operon with 0.5mM IPTG, infected with λ*vir* and the EOP calculated as described in Fig.1B. EOP of λ*vir* for each strain is calculated with respect to the control strain in the same background. The strains used in this experiment are control (DJ624), P_{lac}-*dicBF* (DB240), control *minC* R172A (PR181), P_{lac}-*dicBF minC* R172A

849 (PR183), control *minC* E156A (PR180) and P_{lac}-*dicBF minC* E156A (PR182). Error bars were

850 calculated as standard deviation of values from three biological replicates.

851

852

853

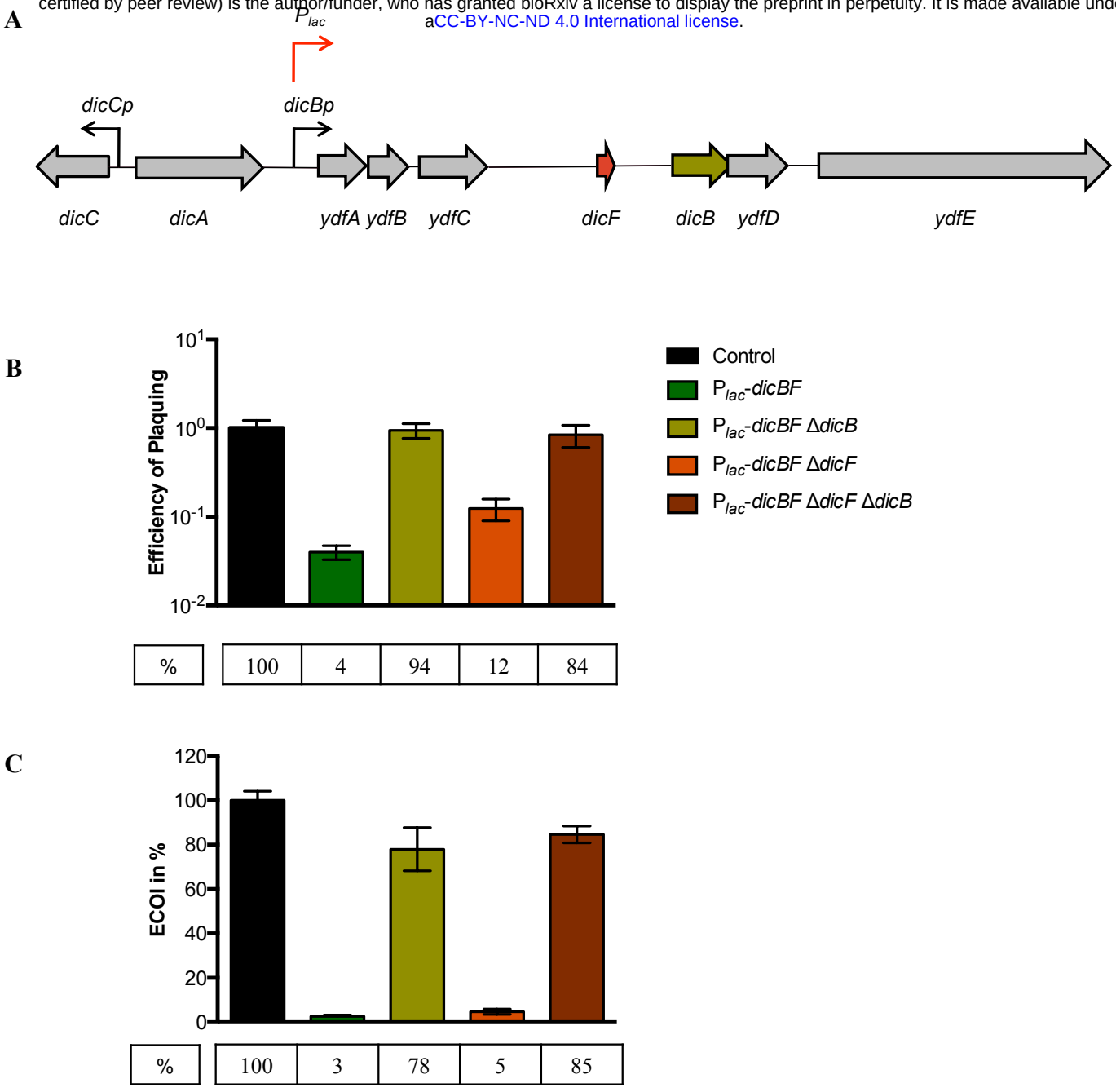

Figure 1. Transient induction of the *dicBF* operon protects against λ*vir* infection. (A) The *dicBF* locus on Qin prophage of *E. coli* K12. The red arrow indicates where P_{lac} is inserted on the chromosome, replacing the native *dicBp* promoter. (B) Efficiency of Plaquing (EOP) is defined as (λ*vir* titer on the test strain)/ (λ*vir* titer on the control strain). Strains used in this experiment were: control (DJ480), P_{lac}-*dicBF* (DB240), P_{lac}-*dicBF* Δ*dicB* (PR165), P_{lac}-*dicBF* Δ*dicF* (DB247) and P_{lac}-*dicBF* Δ*dicF* Δ*dicB* (DB248). All strains were grown to the same state of growth with the *dicBF* operon induced with 0.5 mM IPTG for 60 minutes. The inducer was washed off, the strains were resuspended in TM buffer, infected with λ*vir* and plated to calculate titer. Error bars were calculated as standard deviation of values from three biological replicates. (C) Efficiency of center of infection (ECOI) is calculated as (number of infectious centers/ml from test strain)* 100/(number of infectious centers/ml from control strain). The strains used in this experiment are control (DJ480), P_{lac}-*dicBF* (DB240), P_{lac}-*dicBF* Δ*dicB* (DB243), P_{lac}-*dicBF* Δ*dicF* (DB247) and P_{lac}-*dicBF* Δ*dicF* Δ*dicB* (DB248). The cells were grown with induction of the *dicBF* operon with 0.5 mM IPTG and infected with λ*vir* at an MOI of 0.1. The unadsorbed phages were removed, the phage-host complex was added to phage sensitive cells (DJ480) and plated onto LB agar for counting plaques (infectious centers). Error bars were calculated as standard deviation of values from three biological replicates.

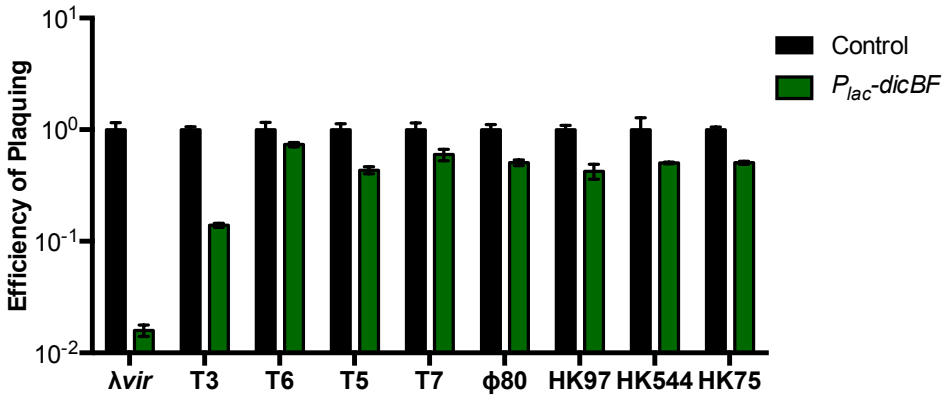

Figure 2. The *dicBF* operon confers resistance against λ phage but not other phages. For each of the nine phages, titer in terms of pfu/ml was calculated by infection of control (DJ480) and P_{lac}-*dicBF* (DB240) cells. The cells were prepared for infection and the EOP was calculated for each phage as described for Fig.1B. Error bars were calculated as standard deviation of values from three biological replicates.

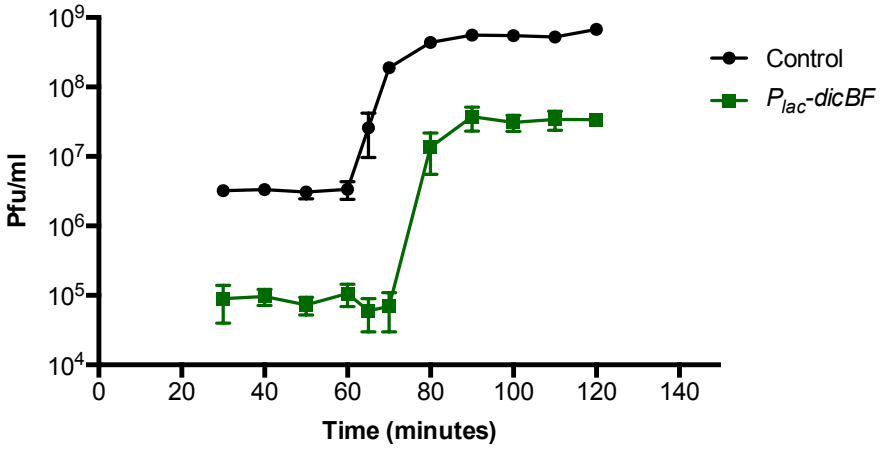

Figure 3. One step growth curve of λ*vir* control and P_{lac}-*dicBF* cells. The cells were grown with induction of the *dicBF* operon and infection was carried out an MOI of 0.1, similar to the center of infection assay. After removing unadsorbed phages, the cells were diluted in LB medium (with IPTG to induce the *dicBF* operon) and incubated at 37°C for the entire duration of the growth curve. At each time point starting at 30 minutes from the start of infection, samples were removed and added to the phage-sensitive strain (DJ480), and plated to count plaques. Burst size was calculated as (phage titer at 100 minutes - initial titer at 30 minutes)/initial titer at 30 minutes. Latent period was calculated as the time at the mid-point of the exponential phase of the curve. Error bars were calculated as standard deviation of values from three biological replicates.

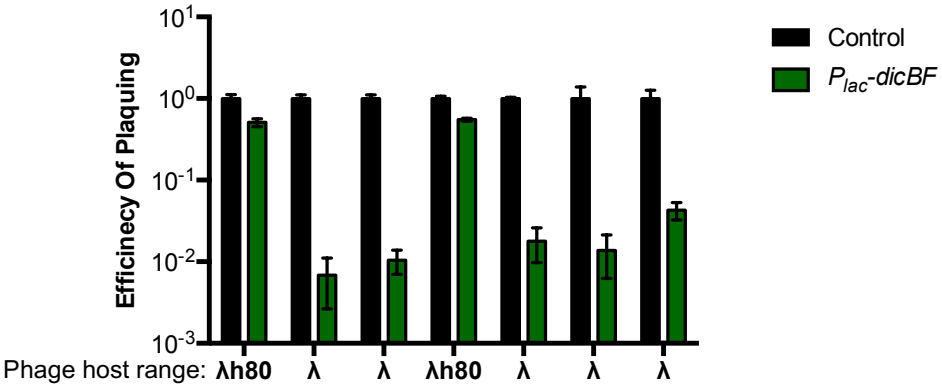

Figure 4. λ phage with the host range of ϕ80 is not affected by DicB. Recombinant λ phages with either the λ or ϕ80 host range were plaqued on control (DJ480) or P_{lac}-*dicBF* (DB240) cells. Phage names from left to right are: 185, 148, 169, 173, 158, 138 and λ*vir* (see Table S1 for phage genotypes). The cells were prepared for infection and the EOP was calculated for each phage as described for Fig. 1B. Error bars were calculated as standard deviation of values from three biological replicates.

A

	λ	434	ϕ80
Outer membrane	LamB	OmpC	FhuA
Inner membrane	ManYZ	ManYZ	TonB

B

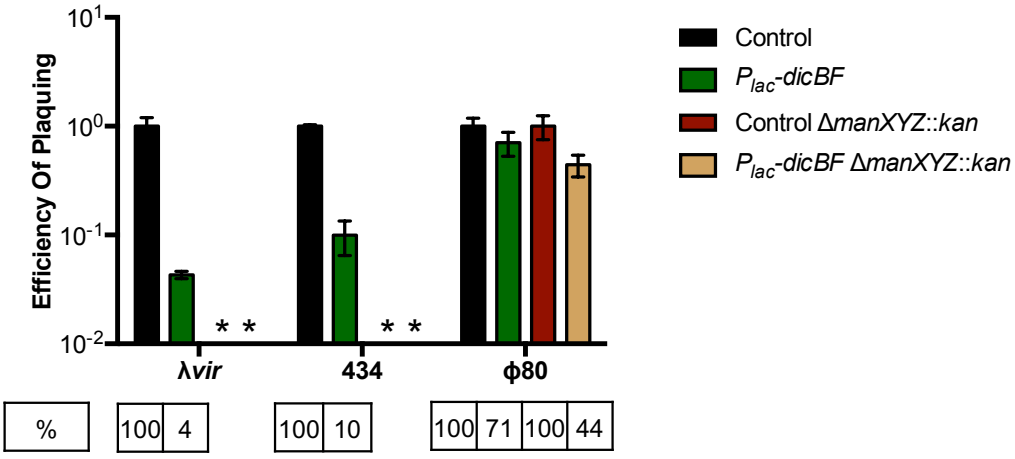

Figure 5. Phage 434 plaquing on ManYZ⁺ strains is inhibited by the *dicBF* operon. (A) Outer and inner membrane receptor specificity of phages λ*vir*, 434 and ϕ80. (B) EOP assay was carried out by preparing cells and calculating titer of phages on the different strains as described in Fig.1B. The strains used in this experiment are control (DJ624), P_{lac}-*dicBF* (DB240), control Δ*manXYZ*::kan (PR187) and P_{lac}-*dicBF* Δ*manXYZ*::kan (PR191). EOP of phages for each strain is calculated with respect to the control strain in the same background. Error bars were calculated as standard deviation of values from three biological replicates. * denotes strains for which plaques could not be counted.

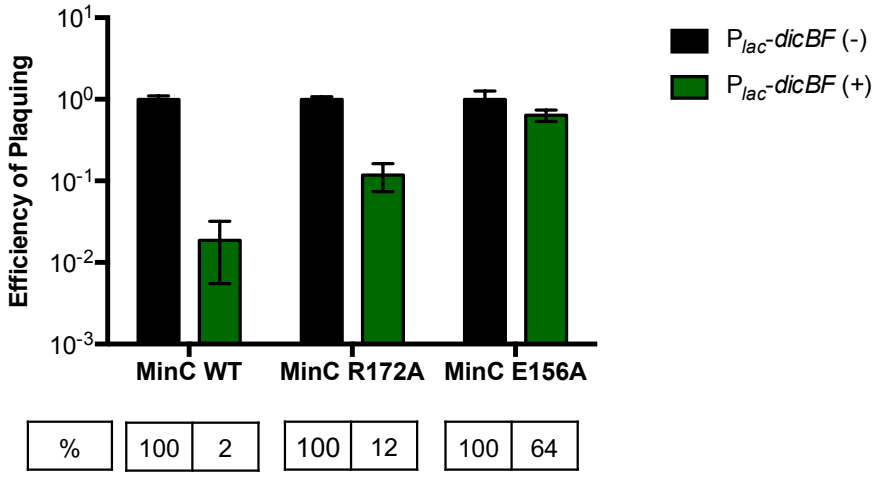

Figure 6. MinC mutants that do not interact with DicB lose the phage resistance effect. The cells were grown with induction of the *dicBF* operon with 0.5mM IPTG, infected with λ*vir* and the EOP calculated as described in Fig.1B. EOP of λ*vir* for each strain is calculated with respect to the control strain in the same background. The strains used in this experiment are control (DJ624), P_{lac}-*dicBF* (DB240), control *minC* R172A (PR181), P_{lac}-*dicBF minC* R172A (PR183), control *minC* E156A (PR180) and P_{lac}-*dicBF minC* E156A (PR182). Error bars were calculated as standard deviation of values from three biological replicates.